# PROPAGATION OF EXCITATION IN IDEALIZED ANISOTROPIC TWO-DIMENSIONAL TISSUE

ROGER C. BARR AND ROBERT PLONSEY
*Departments of Biomedical Engineering and Pediatrics, Duke University, Durham, North Carolina 27706*

ABSTRACT This paper reports on a simulation of propagation for anisotropic two-dimensional cardiac tissue. The tissue structure assumed was that of a Hodgin-Huxley membrane separating inside and outside anisotropic media, obeying Ohm's law in each case. Membrane current was found by an integral expression involving partial spatial derivatives of $V_m$ weighted by a function of distance. Numerical solutions for transmembrane voltage as a function of time following excitation at a single central site were computed using an algorithm that examined only the portion of the tissue undergoing excitation at each moment; thereby, the number of calculations required was reduced to a large but achievable number. Results are shown for several combinations of the four conductivity values: With isotropic tissue, excitation spread in circles, as expected. With tissue having nominally normal ventricular conductivities, excitation spread in patterns close to ellipses. With reciprocal conductivities, isochrones approximated a diamond shape, and were in conflict with the theoretical predictions of Muler and Markin; the time constant of the foot of the action potentials, as computed, varied between sites along axes as compared with sites along the diagonals, even though membrane properties were identical everywhere. Velocity of propagation changed for several milliseconds following the stimulus. Patterns that would have been expected from well-known studies in one dimension did not always occur in two dimensions, with the magnitude of the difference varying from nil for isotropic conductivities to quite large for reciprocal conductivities.

## INTRODUCTION

This paper reports on a simulation of propagation in anisotropic two-dimensional cardiac tissue. Numerical solutions were found to a problem involving excitation in Hodgkin-Huxley membrane in the $x$-$y$ plane with anisotropic media obeying Ohm's law inside and outside the membrane. This problem was of interest for several reasons: (*a*) An earlier project (1) showed that current flow in two-dimensional anisotropic tissue, especially with reciprocal conductivities, was grossly different from that under isotropic conditions, in particular, action currents are not described by the core conductor model (locally). (*b*) An existing theory developed in a series of papers by Muler and Markin (2) predicts theoretical isochrones for anisotropic tissue based on several assumptions; their predictions could be tested in our model. (*c*) Evaluation of the numerical model posed a challenging problem in computer simulation; its solution might be of great value in other two- or three-dimensional simulation problems.

Our goal was to explore propagation from a single stimulus site in two-dimensional tissue of unlimited extent. Conceptually, two-dimensional excitation can be thought of as three-dimensional tissue excited along an infinite line, with no variation along the third dimension. (One can also regard two-dimensional excitation as that of a very thin tissue [lamina] lying in an insulating medium, since this effectively allows no variation in the third dimension.) The two-dimensional case was chosen because (*a*) with anisotropy present, current flow patterns had been shown to be different qualitatively as well as quantitatively from those for one dimension (1), (*b*) we had the Muler-Markin theoretical analysis for comparison for two dimensions, (*c*) although we were expecting markedly different results in two dimensions compared with one dimension, it was unclear to us what would be expected to occur in three dimensions that didn't occur in two, and (*d*) the problem in two dimensions seemed a difficult enough first step given a reasonable limit on computer resources.

Our first objective was to compute isochrones for excitation beginning at a single site for isotropic, equal ratio, nominally normal, and reciprocal anisotropies (the specific meanings are defined below). A second objective was to estimate velocities as a function of position and time for all three cases, to determine how much time must elapse following a stimulus before stable isochrone shapes and velocities are reached. Finally, we wished to compare action potential morphology (voltage vs. time) for different positions with different anisotropies.

## MATHEMATICAL METHODS

### Conductivity Symbols

Symbols used for conductivities, their sums, and their ratios are defined in Table I. Also shown in Table I are the conductivities for the three cases

TABLE I
SYMBOLS USED FOR CONDUCTIVITIES AND THEIR RATIOS*

| Symbols | Values | | |
|---|---|---|---|
| | *I* (isotropic) | *N* (nominal) | *R* (reciprocol) |
| Primary symbols§ | | | |
| $g_{ix}$ intracellular conductivity along x | 0.2 | 0.2 | 0.2 |
| $g_{iy}$ intracellular conductivity along y | 0.2 | 0.02 | 0.02 |
| $g_{ox}$ extracellular conductivity along x | 0.2 | 0.8 | 0.02 |
| $g_{oy}$ extracellular conductivity along y | 0.2 | 0.2 | 0.2 |
| Derived symbols | | | |
| $G_x = g_{ix} + g_{ox}$ | | | |
| $G_y = g_{iy} + g_{oy}$ | | | |
| $G = (G_x G_y)^{1/2}$ | | | |
| $\lambda_x = g_{ox}/g_{ix}$ (note extracellular *g* in numerator) | | | |
| $\lambda_y = g_{oy}/g_{iy}$‡ | | | |

*In millisiemens per millimeter.
‡In the reciprocal examples, λ with no subscript often is used. $\lambda = \lambda_x = 1/\lambda_y$.
§Consistent with "bidomain" models, both intra- and extracellular conductivities are defined on the total space.

that received the most attention from us. These cases were isotropic tissue (*I*), nominal conductivities for normal ventricular muscle (*N*), and conductivities in a reciprocal (*R*) ratio ($\lambda_x = 1/\lambda_y$), usually with $\lambda_x = 0.1$. The normal conductivities correspond, roughly, to experimental data (unfortunately neither extensive nor consistent), summarized in reference 1.

## Hodgkin-Huxley Membrane Theory

Our interest was limited to the simulation of excitation and the evaluation of the resulting propagation pattern in anisotropic tissue sheets; it did not extend to repolarization. Consequently, calculations were based on the original Hodgkin and Huxley model for nerve (3) since it has been demonstrated that there is no major difference in membrane mechanism between nerve and cardiac muscle during excitation (4). Specific equations were taken from Plonsey (5), where transmembrane voltage, $V_m$, is defined as intracellular potential minus extracellular potential, and outward membrane current, $I_m$, is designated as positive, which is consistent with present conventions. These equations as revised are given in Appendix A.

Calculations utilized the Hodgkin and Huxley equation

$$I_m = C_m \frac{\partial V_m}{\partial t} + (V_m - V_K)\, g_K + (V_m - V_{Na})\, g_{Na} + (V_m - V_L)\, g_L. \quad (1)$$

In Eq. 1, (and all work on this project), $V_m$ was defined as zero at rest. (That is, differences from the resting potential are used in evaluating or assigning $V_m$.) Consequently

$$\begin{aligned} V_m(t) &= [\phi_i(t) - \phi_o(t)] - [\phi_i(\text{rest}) - \phi_o(\text{rest})], \\ &= [\phi_i(t) - \phi_i(\text{rest})] - [\phi_o(t) - \phi_o(\text{rest})] \\ &= \Phi_i(t) - \Phi_o(t). \end{aligned} \quad (2)$$

Note that extracellular potentials $\phi_0$ are not assumed to be negligible in comparison with the intracellular potentials $\phi_i$. The units and values of constants used, such as equilibrium potentials $V_K$, $V_{Na}$, and $V_L$, are given in Table II.

## Calculation of Membrane Current, $I_m$

A major aspect of two-dimensional simulations for anisotropic tissue is evaluating the membrane current, $I_m$.

*Equal Anisotropy Ratios.* In earlier work (1), it was shown that the value of $I_m$ at a point *x,y* for two-dimensional anisotropic tissue with equal anisotropy ratios $\lambda_x = \lambda_y$ could be found from the following expression:

$$I_m(x, y) = M_{VA} \cdot I_V(x, y). \quad (3)$$

Note that the case of equal anisotropy ratios along *x* and *y*, i.e., $\lambda_x = \lambda_y$, includes the isotropic case where $\lambda_x = \lambda_y = 1$.

The membrane current per unit volume, $I_V$, is (1)

$$I_V(x, y) = \frac{1}{1 + \lambda_x} \cdot V_2(x, y) \quad (4)$$

with

$$V_2(x, y) = g_{ox} \frac{\partial^2 V_m}{\partial x^2} + g_{oy} \frac{\partial^2 V_m}{\partial y^2} \quad (5)$$

while $M_{VA}$ = membrane volume per surface area. (We chose $M_{VA} = 5 \cdot 10^{-3}$ mm.)

*General Anisotropy (I).* In this case,

$$I_V(x, y) = [I_{V0}(x, y) + I_{V2}(x, y)]. \quad (6)$$

In Eq. 6, $I_{VO}$ is the "self-term" and can be computed as

$$I_{V0}(x, y) = \left\{ -\frac{W_C}{\pi} \arctan\left[(dy/dx)\,(G_x/G_y)^{1/2}\right] + g_{iy}/G_y \right\} V_2(x, y). \quad (7)$$

TABLE II
SYMBOLS FOR CONSTANTS WITH UNITS AND VALUES

| Constants | Values |
|---|---|
| Conductances | $mS/mm^2$ |
| $\bar{g}_K$ | 0.3600 |
| $\bar{g}_{Na}$ | 1.2000 |
| $\bar{g}_L$ | 0.0030 |
| Equilibrium voltages | $mV$ |
| $V_K$ | −12 |
| $V_{Na}$ | 115 |
| $V_L$ | 10.6 |
| Membrane properties | |
| $C_M$ | 0.010 $\mu F/mm^2$ capacitance/area |
| $M_{VA}$ | 0.0050 mm volume/area |

Term $dy/dx$ is the ratio of the $y$ to $x$ lengths of the sides of an element of area around $x,y$. In Eq. 7

$$W_C = 2(\lambda_x - \lambda_y)/[(1 + \lambda_x) \cdot (1 + \lambda_y)]. \quad (8)$$

In Eq. 6 $I_{V2}(x, y)$ is the "distant term" and is computed as

$$I_{V2}(x, y) = \iint_{\substack{x,y \\ \neq x,y}} \cdot W_{CL}(x - x', y - y') \cdot V_2(x', y')\, dx'\, dy' \quad (9)$$

where

$$W_{CL}(x - x', y - y') = \frac{W_C}{4\pi G} \cdot \frac{(x - x')^2/G_x - (y - y')^2/G_y}{[(x + x')^2/Gx + (y - y'))^2/G_y]^2} \quad (10)$$

and the integral excludes the rectangular area accounted for by the self term. Note from Eqs. 3 and 4 that with equal anisotropy ratios, $I_m$ is found from derivatives of $V_m$ at $x,y$. In contrast, in the general case finding $I_m(x,y)$ requires a spatial integration, according to Eqs. 6 and 9.

## NUMERICAL MODEL

In planning the calculations, we considered our maximum resources to be ~1,000 s times $10^7$ operations per second, or $10^{10}$ operations, and ~400,000 bytes of computer storage. The final strategies that we used, especially as related to the calculations of membrane current, organization of the tissue's geometry, and procedure for doing the Hodgkin-Huxley (HH) calculations (3), all reflected our best judgment about how to solve the problem correctly while keeping the computational requirements within these bounds.

### Organization of the Geometry

An idealized two-dimensional tissue surface was divided into elements of area with edge lengths $dx$ and $dy$, as shown in Fig. 1. Lengths $dx$ and $dy$ usually were 100 $\mu$m. At the center of each element was a node. Conceptually, our computational objective was to evaluate potentials and currents at these nodes. When it was necessary to estimate values of functions of $x,y$, such as $V_m$, over the entire surface, we estimated the continuous function from values evaluated at the nodes. Usually we simply assumed variables to be constant within an element and equal to the value at the node. Because node spacing was regular, nodes were tabulated by index 0, 1, ... rather than by $x,y$ coordinate. Excitation began by stimulating the node at 0,0 and propagated from 0,0 in all directions. Note from Fig. 1 that nodes fall exactly on coordinate axes $x$ and $y$ with adjoining elemental squares extended above and below the axis. This arrangement ensures a similar (symmetrical) response from central stimulation in each of the four quadrants so that results for only one quadrant need be examined. The geometry also allows for the reduction of propagation to one or zero dimensions. The extent of the grid along $x$ or $y$ axes was not fixed in advance but varied dynamically as described below.

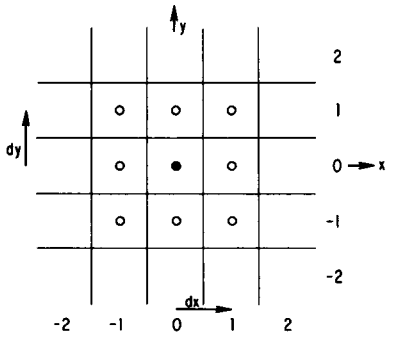


FIGURE 1 Positioning of nodes on $x,y$ grid. The central node (●) was located at the $x,y$ origin. Other nodes (○) were at increments $dx$ and $dy$ in all directions. Usually nodes were identified by specifying values for $i,j$, the node indices, as identified by the numbers on the *bottom* and *right* of the figure.

### HH Computer Procedure

Inspection of the HH equations (3) shows that the state of any node at time $t$ can be characterized completely by specifying the values at that node $V_m(t)$ and HH variables $n(t)$, $m(t)$, and $h(t)$. We tabulated these values for each node.

The sequence of activation of a sheet of tissue was divided into a series of time instants. Thereby, the computational problem deals with the transition from time $t$ to time $t + \Delta t$. Our strategy was to make $\Delta t$ small enough to extrapolate linearly.

Specifically, from the values of $V_m$ at all nodes, a value of $V_2$ and then a value of $I_m$ was found for each node using Eq. 3–10. A spatial integration was required in some cases, as described by Eq. 9. Then, applying Eq. 1 at each node, we used the corresponding values of $n$, $m$, and $h$ along with $I_m$ to estimate $\Delta V$.

Diagramatically,

$$\left.\begin{aligned} V_m(t) &\rightarrow I_m(t) \\ N(t) &\rightarrow g(t) \end{aligned}\right\} \rightarrow \Delta V_m(t). \quad (11)$$

In this diagram, $N(t)$ stands for the values of $n$, $m$, and $h$ at time $t$, while $g(t)$ represents the set of conductivities $g_K$, $g_{Na}$, and $g_L$ at this time.

Similarly, the value of $V_m$ at each node was used to estimate the change in $n$, $m$, and $h$ for that node. Again diagramatically

$$V_m(t) \rightarrow \alpha(t) \rightarrow \Delta N(t). \quad (12)$$

In Eq. 12, symbol $\alpha$ is used to stand for all six rate constants computed using Eq. A5. These rate constants were used to estimate changes in $n$, $m$, and $h$ by Eq. A2.

After both $\Delta V_m(t)$ and $\Delta N(t)$ were found, new values for time $t + \Delta t$ were computed from

$$\begin{aligned} V_m(t + \Delta t) &= V_m(t) + \Delta V_m(t) \\ N_m(t + \Delta t) &= N(t) + \Delta N(t) \end{aligned} \quad (13)$$

where, again, these calculations were done for each node and where $N$ stands for all three parameters $n$ $m$, and $h$ for that node. In the outline above, note that no interaction between different nodes occurs except in computing $I_m$.

Linear extrapolation was used for all calculations, rather than a higher-order or predictor-corrector method. Our judgment favored this choice because (*a*) the linear method provides a good extrapolation as $\Delta t$ approaches zero; moreover, by halving an initial $\Delta t$ we could estimate the residual error; (*b*) our opinion was that the literature showed no order-of-magnitude improvements in time or accuracy in similar problems using more complicated methods; (*c*) it was unclear that it would be profitable to use a predictor-corrector method for $V_m$ unless values of $I_m$, also were predicted and corrected, a lengthy computation since spatial integrations were required for $I_m$, (*d*) already faced with a lengthy and mathematically complicated computer program, we wished to use short, direct methods to make the program easier to read and easier to understand, and (*e*) if a more complicated method were to be used, we would need the linear results for comparison.

## Dynamically Following the Active Region

Our simulation was based on the premise that the behavior of a continuous two-dimensional sheet of cardiac tissue could be approximated by by a discrete grid of nodes separated by short distances. A conventional approach to such a calculation is to fix the dimensions of the tissue and thereby the size of a particular grid of nodes. Thereafter, the transmembrane voltage and other parameters are estimated for the chosen set of nodes for each moment.

Such a procedure would have proved unsuccessful for this problem because the number of calculations would have been too large. Realistic tissue dimensions might have been a square block 10 mm on a side, requiring ~100 nodes per row for 100 rows for a node separation of 0.1 mm, a distance we considered the upper limit of acceptable node spacing. We estimated the number of calculations required using different degrees of approximation (Appendix B). The conclusion we reached was that using a fixed grid of nodes would require computation time in excess of that available.

A marked reduction in the amount of calculation was achieved by using a different strategy, that of dynamically following the active region. This terminology was used to mean keeping track at any moment of only those nodes actively undergoing depolarization. The potential savings of such a maneuver can be envisioned by realizing that in a tissue block 10 mm on a side with a single central stimulus, <10% of the nodes may be actively undergoing depolarization at any moment. The other nodes either are still at rest or have reached their plateau voltage, so that calculations performed for such nodes are unnecessary. Care is required, however, in performing calculations only within the active region since the location of the active region is a consequence of the anisotropic conductivities, and its location as a function of time is not known in advance. Indeed, one of the objectives of the computed results is to determine what it is.

*Times on the Action Potential Waveform.* To follow the active region, it was useful to define and identify four moments that were of special interest in each action potential waveform. These four times, identified individually for each node, are illustrated in Fig. 2.

*Start Time, $T_S$.* Time $T_S$ was defined to be the time when the computer simulation procedure first began consideration of a node. Time $T_S$ was coincident with the beginning of calculations for nodes that were stimulated. Other nodes had a starting time that depended upon active propagation from an immediately adjacent node (see below).

*Propagation Time, $T_P$.* Time $T_P$ was defined to be the time when the transmembrane potential had risen from resting voltage (=0) to voltage $V_P$. In most cases $V_P$ was chosen to be 5 mV. At time $T_P$, "propagation" occurred in the sense that the computer procedure began computing values for the four nodes contiguous along $x$ or $y$ (horizontally or vertically) with the "propagating" node. Time $T_P$ for a given node was equal to time $T_S$ for its four neighbors (unless the neighbors already were active). For example, stimulus node 0,0 orginally propagated to nodes 1,0; 0,1; −1,0; and −0,−1.

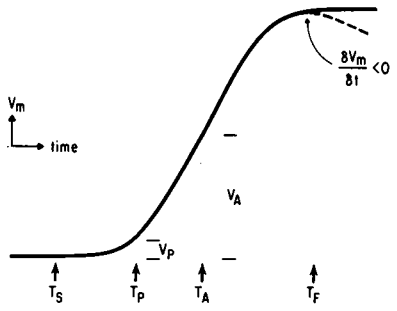


FIGURE 2 Special times on an action potential. For each of the action potentials computed, four particular times were identified. These were the starting time, $T_S$, the propagation time, $T_P$, the activation time, $T_A$, and the finishing time, $T_F$.

*Activation Time, $T_A$.* Time $T_A$ was defined as the time when the transmembrane voltage at a node reached an arbitrarily chosen threshold voltage $V_A$. Time $T_A$ had no significance to the propagation algorithm. It was recorded and later used to draw isochrones showing the activation sequence. $V_A$ usually was chosen to be 50 mV, i.e., ~50% of the upstroke.

*Finishing Time, $T_F$.* Time $T_F$ was defined to be the time when $V_m$ began to repolarize. (Recall that since we used the HH formulation without modification, there was rapid recovery appropriate to nerve.) After $V_m$ reached 90 mV, when a negative change was found, a counter was incremented. The program left voltage $V_m$ unchanged, and subsequent calculation of $I_m$ used the unchanged value. Time $T_F$ occurred when the counter reached three. Because successive iterations of the program ocurred at intervals $\Delta t$, time $T_F$ occurred $2 \cdot \Delta t$ (usually 20 ms) after the action potential first began to repolarize.

This procedure for choosing $T_F$ emerged after a period of trial and error. It was desirable that $T_F$ occur soon after the action potential reached a plateau voltage to keep the number of active nodes low. Conversely, because of the spatial integration for membrane current, second derivatives of $V_m$ computed anywhere affected the current computed for all other nodes. Therefore, it was essential to retain each node long enough to allow accurate computation of the second derivatives between the node and those adjacent, until the derivatives were small. A time delay of two cycles during which $\Delta V_m$ was computed to be negative (although $V_m$ was held constant) allowed time for the derivatives to diminish. (Simulation results showed variations in the plateau values of $V_m$ and in values for $I_m$ to be large enough to discourage choosing $T_F$ from threshold values of $V_m$ and $I_m$.) The method used proved quite satisfactory.

*Sequence of Dynamic Events.* The organization and sequence of events within the simulation program is described in Appendix C. Execution typically began keeping track only of node 0,0. A stimulus current applied to node 0,0 caused $V_m(0,0)$ gradually to rise. When $V_m(0,0)$ reached $V_P$, all nodes adjacent to 0,0 were added to a list of active nodes. As more stimulus current was applied to the central node, $V_m(0,0)$ continued to rise. As the HH events associated with excitation occurred, active propagation began.

Adjacent nodes such as 1,0 were affected by changes at node 0,0 through the $I_m$ calculation; their membrane voltages likewise rose until they also reached $V_P$, adding still more nodes to the active node list. Ultimately, the voltage at 0,0 began to decline and node 0,0 was removed from the active node list; in turn other nodes were removed.

*Calculation of $I_m$ Adjacent to Boundaries.* In computing function $V_2$ at each node, a question of how to form the second differences along $x$ or $y$ arises at each of the several boundaries, namely, (*a*) boundaries identified explicitly beyond which propagation is not allowed, (*b*) boundaries between active nodes and regions still at rest, and (*c*) boundaries between active nodes and nodes no longer active and removed from the list.

Each of these special cases was handled differently. Nodes adjacent to explicit boundaries or tissue at rest were assigned a zero voltage difference between the node adjacent to the boundary and the missing node that would exist across the boundary. This assignment corresponded physically to a requirement that no current flow across the boundary. Nodes adjacent to regions where nodes had been removed after reaching plateau voltage were assigned a voltage difference that was based on the assumption that the plateau region had a fixed voltage, usually 104 mV. This assumption was made whether or not the actual voltage at $T_F$ was

104. Exploration of the numerical results indicated that the effects of inaccuracies in assuming $V_F$ equal to 104 mV at $T_F$ were negligible, probably because node to node variation in computed plateau voltages, while nonzero, was small.

## RESULTS

### Program Validation

Three calculations, described below, showed that our computer procedures, including complexities such as dynamically following the active nodes, were functioning correctly for these cases.

*Zero Dimensions (Nonpropagating).* A stimulus at 0,0 was followed by an action potential at that node, but no propagation to adjacent nodes was allowed. (Derivatives of $V_m$ with respect to $x$ or $y$ were set to 0.) The results were the same as those in the literature for a space-clamped membrane (3).

*One Dimension.* Excitation following a stimulus at 0,0 was allowed to propagate along $x$,0 or $y$,0. Results were close to the values of propagation velocity predicted by Tasaki and Hagawara (6) (Table III, first two rows).

*Two Dimensions, Isotropic Conductivities.* Propagation followed a stimulus applied to the node at 0,0 (Fig. 3). As was expected, the resulting isochrones were circles. The numbers presented on the figure give the number of time intervals that elapsed until time $T_A$ for each node, and may be converted to elapsed time by multiplying by $\Delta t$ (0.01 ms), or to velocities by dividing into the node spacing (0.1 mm). So doing shows that excitation proceeds more slowly at first than later. For example, velocity on the $x$ axis between nodes 2 and 3 is 0.294 mm/ms; velocity rises to 0.435 mm/ms between nodes 7 and 8. The velocity remained unchanged in subsequent intervals, i.e., stability was reached ~0.8 mm from the stimulus site, after ~2.2 ms. In contrast to results below, the sequence of events clearly was not associated with an interaction between the isochrone shape and a spatial integration for $I_m$, since no integration is required for isotropic conductivities.

TABLE III
VELOCITIES ALONG $x$ AXIS ($\theta_x$) AND $y$ AXIS ($\theta_y$)

| | $\theta_x$ | $\theta_y$ | Ratio $\theta_x/\theta_y$ |
|---|---|---|---|
| T/H* | 0.6204 | 0.2089 | 2.97 |
| One dimensional‡ | 0.5967 | 0.2008 | 2.97 |
| Two dimensional, nominal (close)§ | 0.50 ($x$ = 0.3 mm) | 0.18 ($y$ = 0.10 mm) | 2.78 |
| Two dimensional, nominal (far)‖ | 0.5714 ($x$ = 1.4 mm) | 0.1905 ($y$ = 0.44 mm) | 3.00 |

Each line shows the velocities and their ratio in millimeters per millisecond. In § and ‖, the actual distances from the stimulus site are given with each velocity value.
‡ and ‖ are consistent with *, but line § is not.
*Values computed using Tasaki and Hagawara's equation (6).
‡Values found in one-dimensional computer simulations.
§Values found in two-dimensional computer simulations, with nominal anisotropies, close to the stimulus site.
‖Values under the same conditions as §, but further from the stimulus site.

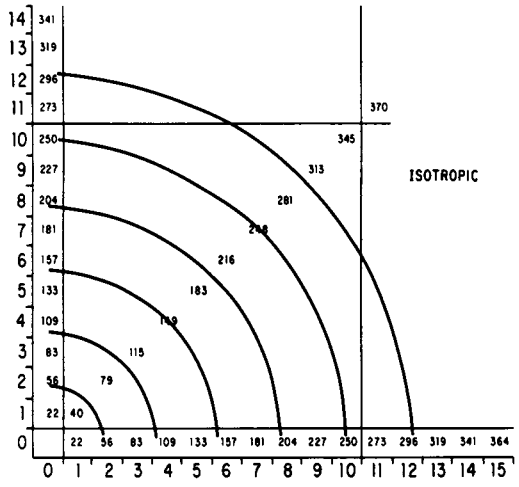


FIGURE 3 Isotropic conductivities. All intracellular and extracellular conductivities were equal, so the simulation was obtained with "equal ratio" form of $I_M$. From the computed values, the number of times steps from the time origin to the activation time ($T_A$) of each node was transcribed onto the grid layout of the figure. The large numbers on the bottom and left indicate the $i,j$ grid indices. They may be converted to the $x,y$ coordinate position by multiplying by d$x$ and d$y$. For clarity in the figure, the time steps are shown only along the $x$ axis, $y$ axis and diagonal, although on the original a time step was present for every node. Further, although the results are shown for one quadrant only, the simulation itself used all four quadrants. (All four were needed to perform the spatial integration for $I_M$.) Isochrones were added manually at multiples of 50 time steps (heavy black lines). As expected, the isochrones were circles. Other straight lines on the grid (lighter black) were added to the figure to make it easier, visually, to judge the relative isochrone positions along $x,y$, and the diagonal; these lines had nothing to do with the calculation. The time origin was chosen arbitrarily to be 0.2 ms after the onset of the stimulus. The time interval from the onset of the stimulus to the activation time of any node can be computed as the number of time steps given on the figure times the interval between steps ($\Delta t$) plus 0.2 ms. Here $g_{ix}$, $g_{ox}$, $g_{iy}$, $g_{oy}$ all equal 0.2 mS/mm; $\Delta t$ = 0.01 ms; d$x$, d$y$ = 0.10 mm.

### Nominal Anisotropy

*Two Dimensions, Self-Term Only.* In these initial calculations, we approximated the integration required for computing $I_m$ by using only the self term, i.e., in Eq. 6 $I_{V2}$ was assumed to be zero. The object of the approximation was to shorten computation time. Conductivity values were chosen to represent those that might be present in normal ventricular muscle (1). The resulting isochrones form a pattern with an oval shape that is similar to patterns seen experimentally. More detailed evaluation showed, however, that computed velocities were high, particularly near the stimulus site, and the approximation was so poor it

had little value. Use of the self-term-only for the reciprocal cases (below) resulted in isochrones that were not even qualitatively correct.

*Two Dimensions, Full Surface Integration.* Our calculations were revised to perform the full surface integration for $I_m$ using both terms of Eq. 6, for nominal anisotropies (Fig. 4). The overall results were computed using values of d$x$ of 0.1 mm and d$y$ of 0.04 mm; portions near the stimulus were confirmed using values of d$x$ and d$y$ of 0.05 and 0.02 mm. Velocities measured along $x$ and $y$ at different distances from the simulus site are shown in Table III.

Close to the stimulus site, velocities along both $x$ (0.50 mm/ms) and $y$ (0.18 mm/ms) axes were lower than predicted by Tasaki and Hagawara for one dimension, as shown in Table III, third row. As propagation progressed further from the site of stimulus, the velocities increased and the discrepency diminished with new values of $\theta_x$ = 0.5714 mm/ms and $\theta_y$ = 0.1405 mm/ms (Table III fourth row).

The closer correspondence came from the changing effect of the spatial integration required to find the membrane current. Because the weighting falls off with distance (Eq. 10), neighboring nodes have a strong effect. In two dimensions, close to the origin the neighboring active nodes are in an elliptical shape; as the ellipse grows, the active neighbors lie more nearly in a straight line. That is, as expected the two-dimensional behavior began to correspond to local one-dimensional propagation asymptotically for large radius.

## Reciprocal Anisotropy

*Two-dimensional Propagation, λ = 0.1.* Initial results (Fig. 5) were computed for a single stimulus at 0,0. Conductivities used for λ = 0.1 were $g_{ix}$ = 0.20 S/mm, $g_{ox}$ = 0.02 S/mm, $g_{iy}$ = 0.02 S/mm, and $g_{oy}$ = 0. 20 S/mm.

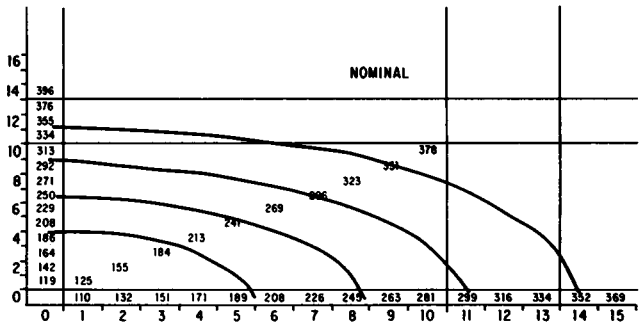


FIGURE 4 Nominal conductivities. Computed times and isochrones for nominal conductivities. The same format as Fig. 3 is used. These elliptical patterns were close but not quite equal to those expected from the Muler-Marken predictions. Here $g_{ix}$, $g_{oy}$ = 0.2, $g_{ix}$ = 0.8, $g_{iy}$ = 0.2, $\Delta t$ = 0.01 ms; d$x$ = 0.10 mm, d$y$ = 0.04 mm.

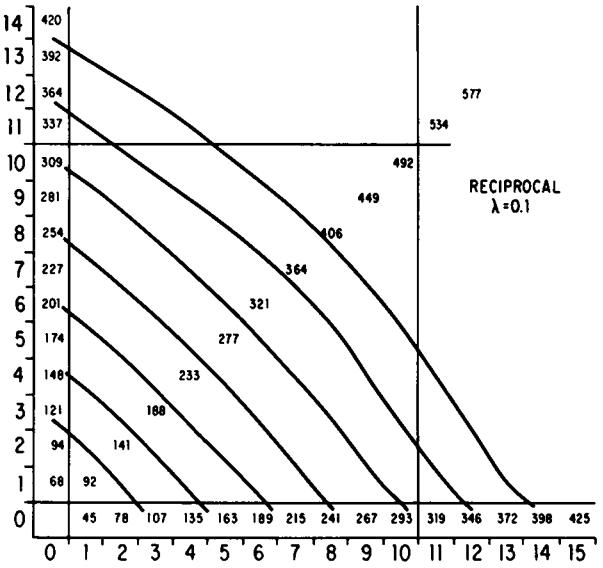


FIGURE 5 Reciprocal conductivities, λ = 0.10. The computed times and isochrones (heavy lines) were markedly different from the shape of isochrones predicted theoretically by Muler and Markin, which more closely approximated the box formed by the lighter straight lines at $i,j$ = 10; presumably the discrepancy occurred because they assumed plane-wave current flow patterns. Same format as Fig. 3. These results were used as a base for comparison to the results following several parameter variations shown in subsequent figures. Note in this and the following figures that excitation times are not precisely symmetric between the $x,y$ axes, a discrepancy that must arise from numerical error. Here $g_{ix}$, $g_{oy}$ = 0.20, $g_{ox}$, $g_{iy}$ = 0.02; $\Delta t$ = 0.01 ms; d$x$,d$y$ = 0.10 mm.

Spatial division along $x$ and $y$ was at 0.10 mm increments. Time steps were 10 μm. The results showed all of the following: (*a*) In segments adjacent to 0,0, propagation along the $x$ or $y$ axis was faster than 45° propagation. (*b*) When propagation reached ~0.5 mm along $x$ or $y$, the shape of the isochrone was between that of a straight line (connecting the 0.5 mm axis crossings on $x$ and $y$) and that of an arc of a circle. (*c*) After ~4 ms, excitation had proceeded ~1.5 mm along and $y$. Excitation bulged out slightly from the straight line connecting the $x$ and $y$ intercepts. (*d*) Away from the immediate vicinity of the excitation point, velocity along $x$ or $y$ was approximately constant and was ≅0.38 mm/ms. Along the 45° line, velocity was approximately constant about 0.34 mm/ms. "Approximately constant" means that the velocities computed from successive pairs of adjacent segments varied slightly, as can be noted from the times given in Fig. 5. These variations were small and probably reflected the numerical approximations of the calculation. (*e*) Resulting isochrones were not consistent with those predicted by Muller-Markin. Those authors predicted the isochrone shape would be similar to that of a square, with sides parallel to the $x$ and $y$ axes. Our isochrones were noncircular in the opposite way, towards a diamond shape. (*f*) The isochrone shapes, which were symmetric in the four quadrants, had their highest curvature at each of the four intersections of axes.

*Variation in the Time Constant of the Foot of the Action Potential (Two Dimensions, λ = 0.1).* The action potentials that were computed at different sites on the two-dimensional grid varied in their time course. The time constant of the foot of the *AP* at a number of sites was found according to the equations given in Appendix D. $K$ values for two dimensions were found to be different from those in one dimension, for the same membrane properties (Table IV). Values of $K$ along the diagonal were greater than those on an axis (Table IV, e.g., node 7,0 compared with node 0,14 or 14,0). Nodes excited earlier had larger $K$ values than later ones. Although numerical errors caused the computed $K$ value to vary from site to site, average $K$ values showed the same trends.

TABLE IV
MEASUREMENTS FOR THE FOOT OF THE ACTION POTENTIAL*

| Time | $I, J$ | $V_m$ | $K$ | $\bar{K}$ |
|---|---|---|---|---|
| *ms* | | | | |
| 0.90 | 0, 6 | 3.5 | — | — |
| | 6, 0 | 2.6 | — | — |
| | 2, 2 | 3.1 | — | — |
| 1.0 | 0, 6 | 4.3 | 2.06 | — |
| | 6, 0 | 3.8 | 3.79 | — |
| | 2, 2 | 6.0 | 6.60 | — |
| 1.10 | 0, 6 | 5.5 | 2.46 | — |
| | 6, 0 | 5.1 | 2.94 | — |
| | 2, 2 | 10.3 | 5.40 | — |
| | | | | (90 → 120) |
| 1.20 | 0, 6 | 6.9 | 2.27 | 2.26 |
| | 6, 0 | 6.7 | 2.73 | 3.16 |
| | 2, 2 | 16.2 | 4.53 | 5.51 |
| 3.00 | 0, 14 | 5.1 | — | — |
| | 14, 0 | 4.0 | — | — |
| | 7, 7 | 1.1 | — | — |
| 3.10 | 0, 14 | 6.3 | 2.11 | — |
| | 14, 0 | 4.9 | 2.03 | — |
| | 7, 7 | 2.4 | 7.80 | — |
| 3.20 | 0, 14 | 7.6 | 1.88 | — |
| | 14, 0 | 6.2 | 2.35 | — |
| | 7, 7 | 4.2 | 5.60 | — |
| 3.30 | 0, 14 | 9.3 | 2.02 | — |
| | 14, 0 | 7.9 | 2.42 | — |
| | 7, 7 | 7.4 | 5.66 | — |
| | | | | (310 → 340) |
| 3.40 | 0, 14 | 11.3 | 1.95 | 1.95 |
| | 14, 0 | 9.9 | 2.26 | 2.34 |
| | 7, 7 | 12.3 | 5.08 | 5.45 |

*Reciprocal anisotropy, λ = 0.1.
Time = elapsed time from time origin; add 0.2 ms for time from start of stimulus. $I, J$ = row and column number of the node. The triplets given for each moment are on the $y$ axis, $x$ axis, and diagonal. $V_m$ = membrane potential. $K$ = time constant of the foot (see Appendix D). For this table, $T^2 - T^1$ was always 0.10 m. The result is shown at $T^2$. $\bar{K}$ = average of the three $K$ values for the interval in parentheses.

Note that the variation in $K$ from node to node occurred even though no variations were present in membrane properties or conductivities from site to site. That is, the $K$ variations were entirely the consequence of differences in the site of the node relative to the stimulus site.

*Two-dimensional Propagation, Four Stimuli (λ = 0.1 Reciprocal Anisotropy), "Star."* As a variation of the excitation conditions above, the tissue was stimulated at four sites symmetrically placed around the origin. Our thought was that if the computer procedures contained some peculiar problem associated with the axes or with simple isochrone shapes, this variation might be qualitatively different from results with one stimulus.

Stimulation occurred simultaneously at four points: 2,2; 2,−2; −2,−2; −2,2. Would propagation from these four points join together to make a squarelike isochrone as the the Muler-Markin theory predicted? It didn't. Instead, there was relatively rapid propagation along $x$ and $y$ from all stimuli. A 12-sided isochrone occurred, with all faces being close to lines at 45° and multiples thereof, or a "star." Some bulging of the sides occurred by 4 ms. Our interpretation was that the same phenomena were occurring for this case as for the single stimulus case.

*λ Variations, Isochrones.* Isochrones were computed for λ = 0.5, 0.3, 0.2, and 0.05. The results demonstrated a smooth transition from the circular isochrones of the isotropic case. Flattening of the sides of the circles became noticeable at λ = 0.2. As λ decreased below 0.1, the isochrones became flatter on the sides, approaching straight lines at 45° angles with the coordinate axes. Fig. 6 shows the isochrones for λ = 0.05.

*λ Variations, Velocities.* Variations in velocity were computed along the diagonal and along the $x$ and $y$ axes with changes in λ (Table V). Also shown are the velocities for one-dimensional propagation that would be predicted by the Tasaki-Hagiwara equation (Appendix D). The values, $\theta_{TH}$, predicted are not consistent with the values of velocity computed in the simulation, either on the diagonal, $\theta_d$, or along $x$, $\theta_x$. That such discrepancies should exist is not too surprising, because the current flow pattern is grossly different in two dimensions compared with that of the one-dimensional preparation for which the equation was derived.

## Solution Stability

Because a lengthy and complicated series of numerical operations was required for each simulation, we tested the stability of some of the computed results by recalculating them after changes that should have been inconsequential. Stability was tested for the reciprocal case, a case with no

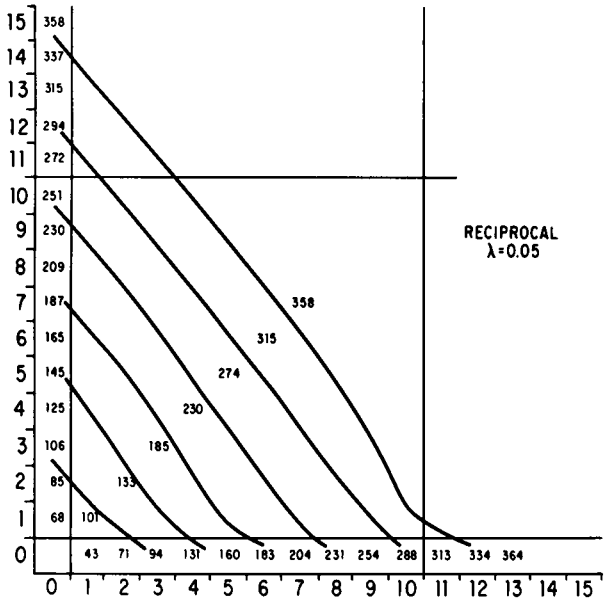


FIGURE 6 Reciprocal anisotropy, $\lambda = 0.05$. Isochrones for reciprocal anisotropy even more extreme than Fig. 5. A smooth transition occurred between this pattern and the isotropic pattern with changes in $\lambda$. Same format as Fig. 3. Here $g_{ix}$, $g_{oy} = 0.20$, $g_{ox}$,$g_{iy} = 0.01$; $\Delta t = 0.01$; d$x$,d$y$ = 0.10.

analytical or measured results for comparison. We also thought that reciprocal anisotropy, as an extreme case, would be more sensitive to perturbations.

*Change of Time Step, $\Delta t$.* The original time step was 10 $\mu$s. New results were computed for a time step of 5 $\mu$s (Fig. 7) and 2 $\mu$s. Minor changes in quantitative results were observed with almost no change in isochrone shape.

*Change of Voltage Threshold for "Propagation," $V_p$.* In dynamically following the active region, the program examined each node's voltage. When the voltage reached $V_p$, the program began to examine all surrounding nodes (above). We were concerned that the solution might vary with changes in $V_p$, since currents of small magnitude flow for some distance ahead of the advancing excitation wave. No effects of these currents were computed in those regions where the membrane voltage had not yet reached

TABLE V
VELOCITY TABULATION FOR DIFFERENT VALUES OF $\lambda$—RECIPROCAL CONDUCTIVITIES

| Case | $\lambda$ | $g_{ix}$ | $g_{ox}$ | $r_x = (1/g_{ix} + (1/g_{ox})$ | $\theta_{TH}$ | $\theta_d$ | $\theta_x$ |
|---|---|---|---|---|---|---|---|
| 1 | 0.5 | 0.1 | 0.1 | 15 | 0.4 | 0.371 | 0.364 |
| 2 | 0.3 | 0.06 | 0.06 | 21.67 | 0.33 | 0.336 | 0.313 |
| 3 | 0.2 | 0.04 | 0.04 | 30.0 | 0.28 | 0.328 | 0.294 |
| 4 | 0.1 | 0.02 | 0.02 | 55.0 | 0.21 | 0.328 | 0.385 |
| 5 | 0.05 | 0.01 | 0.01 | 105.0 | 0.15 | 0.328 | 0.401 |

$\theta_{TH} = \theta$ predicted. (See Appendix D.)
$\theta_d$ = estimated from time differences along a 45° line.
$\theta_x = \theta$ computed from time differences along $x$.

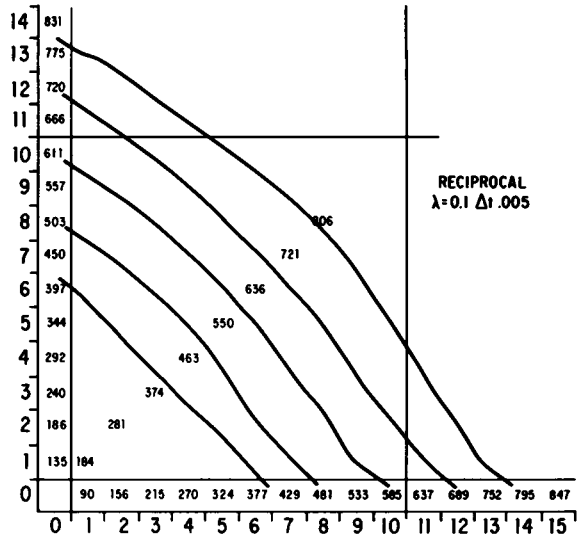


FIGURE 7 Reciprocal conductivities, reduced time intervals. Isochrones were recomputed with $\Delta t$ reduced from 10 to 5 $\mu$s. Comparison with isochrones of Fig. 5 showed little change, except, of course, that the number of time steps here corresponded to half the number there, for the same time interval. Here $\lambda = 0.1$, $g_{ix}$, $g_{oy} = 0.20$, $g_{ox}$, $g_{iy} = 0.02$; $\Delta t = 0.005$; d$x$,d$y$ = 0.01.

$V_p$ mV. Originally, $V_p$ was 5 mV. We compared the original with results for $V_p$ of 2 mV. The magnitudes of changes was small, even in comparison with the changes arising from the smaller time step. However, with $V_p = 2$ mV the calculation took about 50% longer since ~25% more nodes were being considered during each interval.

*Variation in the Size of Each Geometric Element.* This change produced the largest effect in the computed result (Fig. 8). In the original calculation, the

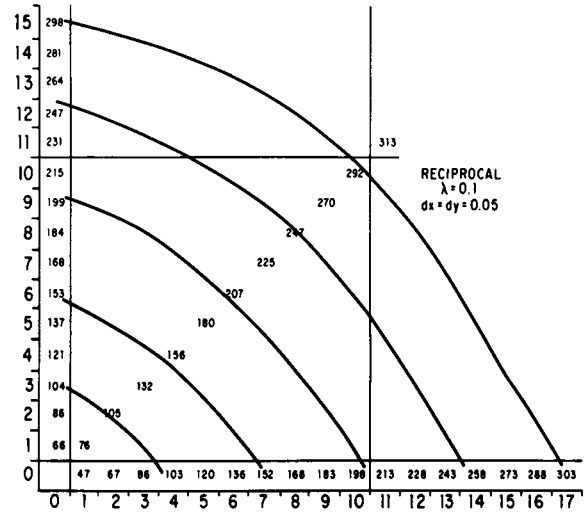


FIGURE 8 Reciprocal conductivities, smaller grid elements. Isochrones computed with reciprocal conductivities, $\lambda = 0.1$, and with the edge length of each segment of the grid reduced by one half. The isochrones shown are much closer to circles than those of Fig. 5, although still not circular. Here $g_{ix}$, $g_{oy} = 0.2$, $g_{ox}$, $g_{iy} = 0.02$; $\Delta t = 0.01$; d$x$,d$y$ = 0.05.

continuous two-dimensional sheet was divided into segments 100 $\mu$m on a side. Significant voltage and current changes occurred within this distance; however, this discretization was retained to minimize the number of nodes carried forward at each step, because $N_g$ was the most important parameter in determining the length of the calculation. We recomputed part of the results with elements 50 $\mu$m on a size (resulting in four times as many elements at each moment). This change increased the computation time by a factor of 16. There was a noticeable change in the results, with isochrones becoming more rounded, although still not circular.

## DISCUSSION

Previous studies on two-dimensional anisotropic tissue are few in number. Plonsey and Rudy (7) and Plonsey and Barr (1) assumed isochrones of particular (reasonable) shapes and concentrated interest on resulting currents and potential fields. In the work of Spach et al. (8) the initial isochrone shapes were determined experimentally and, using a source-field model, formed the basis of calculation of extracellular fields. Also, since the thin tissue was placed in a tissue bath, the interstitial anisotropy was greatly modified and could be taken to be isotropic (9). Except for the theoretical study of Muler and Markin (2), which has already been commented on, only the work of Joyner et al. (10) has as its goal a determination of isochrone shape based on Hodgkin-Huxley two-dimensional membrane. In this work, however, the interstitial (extracellular) space has infinite conductivity so that an equal anisotropy ratio is implied. The resulting isochrones are similar to those shown here in Figs. 3 and 4. Joyner et al. also note an initially increasing velocity to a steady-state value.

Some of the points shown by this series of calculation are that (*a*) it is practical to compute two-dimensional propagation sequences for ventricular muscle sheets with general anisotropic conductivities. The calculation requires that an integral expression be evaluated for $I_m$. (*b*) The most important factor controlling the length of calculation was found to be the number of nodes in the grid, $N_g$. Calculation time increased with $N_g$. To decrease this time, $N_g$ was reduced by considering only that portion of the grid in the active state, i.e., the portion where $V_m$ was changing, carrying forward at each moment only information about the nodes in that region. (*c*) Even with the calculation time reduced by reducing $N_g$, the length of the calculation used almost all our available resources. For this reason, the length of the sides of elements in the grid, d$x$ and d$y$, was chosen to be 100 $\mu$m for most calculations. (For comparison, when d$x$ and d$y$ were reduced to 50 $\mu$m, $N_g$ increased by a factor of 4, and the calculation time increased by 16.) We considered the side length of 100 $\mu$m to be near the upper boundary of acceptable choices, since previous work (1) showed significant changes in current magnitudes within that distance. Further, the results here showed changes in the isochrone patterns using d$x$ and d$y$ values of 100 $\mu$m vs. 50 $\mu$m, as seen by comparing Figs. 5 and 8, although major features of the results remained the same. Other results, such as the time constants for the foot of the action potential shown in Table IV, may have been affected to an unknown degree by d$x$ and d$y$ being larger than desirable.

(*d*) Results for two dimensions with isotropic conductivities or with conductivity ratios equal along $x$ and $y$ were found to be consistent with those expected analytically and to have characteristics (such as velocity) consistent with those expected from one-dimensional analytical results.

(*e*) Isochrones for two dimensions with nominal conductivities (those of ventricular muscle, approximated from the limited experimental data summarized in reference 1) were approximately elliptical and consistent with the Muler-Markin theoretical predictions (within the precision of our calculations) once excitation moved away from the stimulus site.

(*f*) Results for reciprocal conductivities along $x$ and $y$ with $\lambda = 0.10$ diverged markedly from those predicted by Muler-Markin. Isochrones approximated a diamond shape (with the corners on the axes) rather than the square shape (with corners on diagonals) predicted by the Muler-Markin theory. This discrepancy is perhaps not surprising since the Muller-Markin result assumes plane-wave behavior at each element of isochrone. At least for the radius of curvature in the simulations reported here, such plane wave behavior does not occur (1); in fact, the pattern of currents is quite different. Whether the asymptotic behavior described by Muller-Markin would ever be reached cannot be judged from our calculations because of their limited time duration. However, asymptotic agreement between Muler-Markin and our calculations, if extended, is doubtful since the current flow pattern is being strongly affected by the conductivities of the medium itself as well as the shape of the isochrone.

(*g*) For reciprocal conductivities, the shapes of action potentials varied, particularly for points along the axes compared with points along the line at 45°. Apparent velocity also varied. Values were different from those expected from the one-dimensional analysis of Tasaki-Hagiwara. The time constant of the foot was not constant from place to place.

(*h*) The time from the stimulus until the isochrones reached a stable shape could not be defined completely because of the limited time duration of the simulation and numerical noise in the results. However, substantial variation in apparent velocity (though not in shape) was observed in the first few milliseconds; thereafter changes were small. Technically, the basis for the variation appeared to be the integral expression for $I_m$, since this calculation formed the only interaction between elements. From a physiological perspective, that the variation in $I_m$ leads to the other changes seems plausible, and, if not supported in detail by experimental work we could cite, was at least not contradictory to it. For one and two-

dimensional modeling (equal anisotropy) similar conclusions have been noted elsewhere (10,11).

(*i*) The results for reciprocal conductivity varied smoothly with λ. For (10,11) λ of 0.5 or greater, the isochrones were almost circles. For λ = 0.2, there were visual differences from circles. At = 0.05, the sides appeared close to flat.

(*j*) Results of the calculations were largely unaffected by shortening $\Delta t$ below 10 μs, or decreasing the threshold potential from 5 to 2 mV. Decreasing the size of each geometric element of the surface from edges of 100 μ to edges of 50 μm made the isochrones more nearly round.

(*k*) At least for extremely anisotropic tissue, the results depend to a marked degree on current flow patterns that have no corollary in one dimension, giving rise to largely unexplored two-dimensional effects.

## Conclusions

This paper has described a computer simulation for exploring excitation of two-dimensional cardiac tissue possessing general intracellular and extracellular anisotropies. Though actual cardiac excitation often occurs in active tissue regions of two and three dimensions that are anisotropic, the understanding of such excitation is largely based on mathematical relationships and experimental findings obtained for one dimension. At least in some respects, the simple extension of such one-dimensional results to two dimensions was found to be incorrect. For example, the absence of plane wave relations, at least in the early period, invalidates approaches using that approximation, e.g., the predictions of Muler and Markin. More generally, there were substantial variations in two dimensions from well-known relationships established in one dimension. For example, there was not a constant relationship between the time constant of the foot of the action potential (*K*) and the apparent velocity, and velocity itself varied depending on the distance from the stimulus site and the apparent direction of propagation, even though no variation existed in the (idealized) tissue properties from site to site. The magnitude of the differences between two-dimensional results and those expected from established one-dimensional results varied from nil for isotropic tissue to quite large for reciprocal anisotropies having intracellular $x$ and extracellular $y$ conductivities much larger than extracellular $x$ and intracellular $y$ values. Actual cardiac tissue properties lie between these two extremes and must therefore exhibit some combination of the functional characteristics of one-dimensional excitation combined with those characteristics unique to anisotropic media of two or three dimensions.

## APPENDIX A

In Eq. 1, conductivities $g_K$, $g_{Na}$, and $g_L$ are defined (according to Hodgkin-Huxley [3]) by

$$g_K = \bar{g}_K n^4$$
$$g_{Na} = \bar{g}_{Na} m^3 h$$
$$g_L = \bar{g}_L \qquad \text{(A1)}$$

where $g_K$, $g_{Na}$, and $g_L$ are constants (Table II) and the parameters $n$ $m$, and $h$ are defined by Eq. A2 as follows

$$\frac{dn}{dt} = \alpha_n(1 - n) - \beta_n n$$
$$\frac{dm}{dt} = \alpha_m(1 - m) - \beta_m m$$
$$\frac{dh}{dt} = \alpha_h(1 - h) - \beta_h h. \qquad \text{(A2)}$$

If the membrane patch has been at rest for a long time then $\alpha_n$ and $\beta_n$ are at their resting value, so that, from Eq. A2 with $dn/dt = 0$, we have

$$\alpha_n(1 - n_o) - \beta_n n_o = 0; \qquad n_o = \alpha_n/(\alpha_n + \beta_n). \qquad \text{(A3)}$$

Similarly, initial conditions $m_o$ and $h_o$ are given by

$$m_o = \frac{\alpha_m}{\alpha_m + \beta_m} \qquad h_o = \frac{\alpha_h}{\alpha_h + \beta_h}. \qquad \text{(A4)}$$

Initially (at rest) $n$, $m$, and $h$ have the values $n_o$, $m_o$, and $h_o$ (Eqs. A3, A4). The evolution of $n$, $m$, $h$ is according to differential equations (Eq. A2). In Eqs. A2 and A3, the alphas and betas are rate constants determined, for the squid axon, to be

$$\alpha_n = \frac{0.01(10 - V_m)}{\exp[(10 - V_m)/10] - 1}$$
$$\beta_n = 0.125 \exp - \frac{V_m}{80}$$
$$\alpha_m = \frac{0.1(25 - V_m)}{\exp[(25 - V_m)/10] - 1}$$
$$\beta_m = 4 \exp - \frac{V_m}{18}$$
$$\alpha_h = 0.07 \exp - \frac{V_m}{20}$$
$$\beta_h = \left[\exp\left(\frac{30 - V_m}{10}\right) + 1\right]^{-1}. \qquad \text{(A5)}$$

## APPENDIX B

## Estimates of the Computer Time

The length of time required for a complete HH simulation of excitation in two dimensions was estimated using the following definitions:

- $T_0$ time required for one computer operation
- $N_g$ number of nodes in the grid
- $N_H$ number of operations required to go from one time instant to another at a single node for the HH variables $V_m$ and $n$, $m$, and $h$
- $N_M$ number of miscellaneous operations required to go from one time instant to another for a single node
- $N_t$ number of time instants considered for one complete simulation

$N_{IS}$ number of operations required to find the self term of $I_m$ at a single node

$N_{ID}$ number of operations required to find the contribution to the distant term of $I_m$ for a single distant element with respect to a single node.

Values were found for the following derived quantities:

$T_p$ time required for one complete simulation

$N_I$ number of operations required to find $I_m$ at a single node

$N_p$ number of operations required for the simulation

$N_t$ number of operations required for one time step.

As used above, "operation" means an arithmetic operation such as multiplication, including whatever internal computer functions are needed to evaluate subscripts, access the appropriate operands, load and store registers, etc. Because our interest was in order-of-magnitude estimates, a precise definition was not necessary.

For the entire simulation

$$T_p = N_p \cdot T_o \tag{B1}$$

where

$$N_p = N_t \cdot N_I. \tag{B2}$$

A single time step has $N_t$ operations, where

$$N_I = N_g \cdot (N_I + N_H + N_M). \tag{B3}$$

A critical factor is the number of steps to find $I_M$,

$$N_I = N_g \cdot N_{ID} + N_{IS}. \tag{B4}$$

Using Eqs. B4 and B3 in Eq. B2 gives

$$N_p = N_t \cdot [N_g \cdot (N_g \cdot N_{ID} + N_{IS} + N_H + N_M)] \tag{B5}$$

which can be written as

$$N_p = N_g^2 (N_t \cdot N_{ID}) + N_g N_t \cdot (N_{IS} + N_H + N_M) \tag{B6}$$

or, finally, using Eq. B6 in B1

$$T_p = T_o \cdot [N_g^2 N_t N_{ID} + N_g N_t (N_{IS} + N_H + N_M)] \tag{B7}$$

Eq. B7 was the basis for our estimates. Note that in Eq. B7 $N_g^2$ appears in the left term along with $N_{ID}$ because of the spatial integration to find $I_m$ at each node.

*Examples of Estimates.* In all the following estimates, a value of 100 has been used for $N_H$, $N_M$, and $N_{IS}$. Additionally, the "time per operation" $T_o$, has been chosen as $10^{-7}$ s per operation, an estimate based on measured program executions on the IBM 370/165 or Amdahl 470/V8 at Triangle Universities Computation Center (TUCC), Research Triangle Park, NC.

*Example 1 (Brute Force).* In this example, we chose a moderately conservative value for each parameter. $N_{ID} = 100$ (i.e., for the $I_m$ surface integration), $N_g = (10 \text{ mm}/10\ \mu\text{m})^2 = 10^6$ nodes on a 10 mm$^2$ tissue block, and $N_t = 10^4$ steps (10 ms at 1 $\mu$s intervals). These values result in

$$\begin{aligned} T_p &= 10^{-7} [10^{12} \cdot 10^4 \cdot 10^2 + 10^6 \cdot 10^4 (3 \cdot 10^2)] \\ &= 10^{-7} (10^{18} + 3 \cdot 10^{12}) \approx 10^{12} \text{ s} \approx 3{,}000 \text{ y}. \end{aligned} \tag{B8}$$

Because of uncertainty about the long-term stability of the social security system, we chose not to attempt this calculation. The factor contributing most to this estimate is the large number ($10^6$) of nodes.

*Example 2 (Self-Term Only).* In this example, we retained the number of nodes $N_g = 10^6$ and $N_t = 10^4$, but changed $N_{ID}$ to 0 since no integration over a distant region was postulated:

$$\begin{aligned} T_p &= 10^{-7} [10^{12} \cdot 10^4 \cdot 0 + 10^3 \cdot 10^4 (3 \cdot 10^2)] \\ &= 10^{-7} (3 \times 10^9) = 300 \text{ s} = 6 \text{ min}. \end{aligned} \tag{B9}$$

Note the dramatic reduction, in spite of having one million nodes. This example applies to problems with equal anisotropy ratios (including isotropic), and shows those situations to require calculations of moderate length. (However, a self-term only approximation was found to be grossly wrong, generally.)

*Example 3 (Restricted).* In this example we chose a much smaller value for $N_g$ of 500 because of the strong impact of $N_g^2$ on the number of operations. Additionally, we chose $N_t = 1{,}000$ (1 ms at 1 $\mu$s intervals or 10 ms at 10 $\mu$s intervals), a shorter but informative interval. Finally, $N_{ID} = 100$ reflected the necessity of spatial integration. The resulting time was

$$\begin{aligned} T_p &= 10^{-7} [(5 \cdot 10^2)^2 \cdot 10^3 \cdot 10^2 + \\ &\quad 5 \cdot 10^2 \cdot 10^3 (3 \cdot 10^2)] \\ &= 10^{-7} (2.5 \cdot 10^{10} + 1.5 \cdot 10^8) \simeq 2{,}500 \text{ s} \simeq 42 \text{ min}. \end{aligned} \tag{B10}$$

This calculation was considered to be lengthy but achievable. The relatively short time interval simulated by $N_t$ still allowed us to focus on the time of maximum interest, the initiation of propagation following a stimulus up to the time of a stable isochrone shape. The principal limitation was the low value of $N_g$ of only 500. This minimum value was selected after considering an excitation wave of 1 mm thickness represented by nodes at 100 $\mu$m intervals, propagating in a circle away from the origin with the leading edge at $r = 1$ mm while the trailing edge was at $r = 0$, giving a value of 314 nodes as a lower bound on the number of nodes in the active region.

We did not think it was acceptable to restrict our attention to such a small region (and time) following a stimulus, although the length of calculation of 42 min with only 500 nodes showed we could not allow $N_g$ to increase by much. Therefore, we adopted the plan of dynamically following the nodes in the active region.

In that plan, the number of nodes increases gradually from one to its final value. In our calculations the final value was ~700. As expected geometrically and confirmed by calculation, once excitation began, the number of active nodes increased linearly with elapsed time, to a good approximation. (Eq. B7 is readily modified to reflect the changing values of $N_g$).

## APPENDIX C

## Organization of the Simulation Program, HHA

The functions of the main program were divided into subroutines that were used sequentially. The most important of these were routines (*a*) to compute the spatial derivatives, (*b*) to perform the Hodgkin-Huxley calculation, (*c*) to compute the membrane currents by spatial integration, and (*d*) to determine when propagation should occur to adjacent nodes.

*Boundaries of Propagation.* An advantage to dynamically following the active region is that trying to anticipate what the shape of the active region will be at the end of the simulation is neither necessary or advantageous, because nodes will be added to the active list in the right way for whatever shaped region occurs.

Nevertheless, parameters limiting the extent of propagation along each axis in the positive and negative directions were included. These

were designated NNXP (number of nodes on $x$ in the positive direction), NNXN, NNYP, and NNYN.

Boundaries were useful because they allowed the same program to solve problems in zero, one or two dimensions. Setting NNXP, NNXN, NNYP, and NNYN all to zero produces a membrane action potential on element 0,0. Similarly, setting NNYP, NNYN to zero allows an examination of propagation along the $x$ axis, i.e., in one dimension. Care had to be exercized in specifying boundaries, since the theory for computing the membrane current for two-dimensional tissue (with general anisotropy parameters) assumes that the tissue is infinite in extent.

## APPENDIX D

Methods used for finding time constants and predicted velocities. In finding the time constants, the shape of the foot of the action potential was assumed to be exponential according to the equation

$$V_m = Ae^{Kt} \tag{D1}$$

where $V_m$ is the membrane potential and $A$ and $K$ are assumed constant. $K$ was computed from the values of $V_m$ at two times ($V_m^1$ and $V_m^2$ at times $T^1$ and $T^2$) by the equation

$$K = \frac{\ln V_m^2 - \ln V_m^1}{T^2 - T^1}. \tag{D2}$$

Predicted velocities were computed from the Tasaki-Hagawara formula (6) given by

$$\theta_{TH} = \left[\frac{4.8\ \text{ms}^{-1}}{2\left(\frac{1}{g_{ix}} + \frac{1}{g_{ox}}\right)}\right]^{1/2} = \left(\frac{2.4}{r_x}\right)^{1/2}. \tag{D3}$$

The value of 4.8 $\text{ms}^{-1}$ in the numerator was obtained by choosing the value that was the best fit to the computed waveform propagating in one dimension.

This paper was supported by U. S. Public Health Service grants HL11307, HL17931, HL06128, through the National Institutes of Health.

*Received for publication 21 July 1983 and in final form 13 November 1983.*

## REFERENCES

1. Plonsey, R., and R. C. Barr. 1984. Current flow patterns in two-dimensional anisotropic bisyncytia with normal and extreme conductivities. *Biophys. J.* 45:557–571.
2. Muler, A. L., and V. S. Markin. 1978. Electrical properties of anisotropic nerve-muscle syncytia. III. Steady form of the excitation front. *Biophysics.* 22:699–704.
3. Hodgkin, A. L., and A. F. Huxley. 1952. A quantitative description of membrane current and its application to conductance and excitation in nerve. *J. Physiol. (Lond.).* 117:500–544.
4. Ebihara, L., N. Shigeto, M. Lieberman, and E. A. Johnson. 1980. The initial inward current in spherical clusters of chick embryonic heart cells. *J. Gen. Physiol.* 75:437–456.
5. Plonsey, R. 1969. Bioelectric Phenomena. McGraw-Hill, Inc., New York.
6. Tasaki, I., and S. Hagawara. 1957. Capacity of muscle fiber membrane. *Am. J. Physiol.* 188:423–429.
7. Plonsey, R., and Y. Rudy. 1980. Electrocardiogram sources in a two-dimensional anisotropic activation model. *Med. Biol. Eng. Comp.* 18:87–94.
8. Spach, M. S., W. T. Miller III, E. Miller-Jones, R. B. Warren, and R. C. Barr. 1979. Extracellular potentials related to intracellular potentials during impulse conduction in anisotropic canine cardiac muscle. *Circ. Res.* 45:188–204.
9. Geselowitz, P. B., R. C. Barr, M. S. Spach., and W. T. Miller III. 1982. The impact of adjacent isotropic fluids on electrograms from anisotropic cardiac muscle. *Circ. Res.* 51:602–613.
10. Joyner, R. W., R. Ramon, and J. W. Moore. 1975. Simulation of action potential propagation in an inhomogeneous sheet of coupled excitable cells. *Circ. Res.* 36:654–661.
11. Kootsey, M., and E. A. Johnson. 1980. The orgin of the T-wave. *CRC Crit. Rev. Bioeng.* 5:233–270.